European Journal of Clinical Pharmacy

Print ISSN: 2385-409X **Online ISSN:** 3105-0409

Website: https://farmclin.es/

Original Research Article

Synthesis, Characterization, Dye Degradation and Microbiological Activity of Activated Charcoal Supported Cadmium Doped SnO_2 Nano Clusters by Precipitation Method

Article History:

Name of Author:
S. Gunavathi[1], K. Arulvani[2]*

Affiliation: *[1]Associate Professor, Department Of Chemistry, Thiru Kolanjiappar Govt. Arts College, Vridhachalam.606 001, shanma.guna@gmail.com*

[2]Associate Professor, Department Of Chemistry, Thiru Kolanjiappar Govt Arts College Vridhachalam.606 001, vaniramji83@gmail.com*

Corresponding Author: K. Arulvani
Email: *vaniramji83@gmail.com*

Received: 10/11/2025
Revised: 28/11/2025
Accepted: 14/12/2025
Published: 26/12/2025

Abstracts: In the present work, SnO_2, Cd/SnO_2 and AC-Cd/SnO_2 nanoclusters were prepared using precipitation method. The synthesized samples were characterized using X-ray powder diffraction (XRD), high resolution scanning electron micrographs (HR-SEM) with energy dispersive X-ray analysis (EDX), photoluminescence (PL) UV-Vis diffuse reflectance spectroscopy (DRS) and Fourier transform Raman analysis (FT-RAMAN). The XRD and SEM studies reveal that the synthesized SnO_2 nano materials have hexagonal wurzite structure with average crystalline size ~28 nm. Photocatalytic activity under ultra violet (UV) light exposure has been studied using methylene blue (MB) dye as test contaminant. A possible mechanism is proposed to explain the charge carrier recombination and interfacial charge transfer processes. It has been found the optimum amount of Cd^{2+} doping and increased adsorption ability of light due to high separation rate of photo induced charge carriers, which play an important role enhancing the overall photo catalytic performance significantly. Further its antibacterial activity against two gram positive and two gram negative bacterial strain and Antifungal also studied.

Keywords: Ac-Cd/SnO_2 Nanocomposite, Precipitation method, Characterization, Photo degradation, Microbiological activity

INTRODUCTION

Textile industries produce extensive volume of coloured effluents. Among the different types of dyes used in industries, 65-75% belongs to azo compounds. The release of these coloured dyes in the ecosystem without treatment creates extreme environmental pollution problem by releasing toxic and potential carcinogenic substances into the aqueous phase and damaging to the aesthetic nature of the environment [1]. Many traditional techniques such as precipitation, adsorption, air stripping, reverse osmosis, ultra filtration and coagulation have been utilized so far the waste water treatment but they lost their vitality due to

usually nondestructive nature towards target molecules and they generate auxiliary pollutants of transferring contaminants from water to another phase [2] Hence it is important to develop treatment methods that are more viable in destructing dyes from waste water. The removal of azo-dyes by advanced oxidation processes (AOPs) has been the subject of several recent studies. The mechanism of dye destruction in AOPs is based on the formation of a extremely reactive hydroxyl radical (•OH), that, with an oxidation potential of 2.80V can oxidize a broad range of organic compounds [3]. Photocatalysis, as a "green" technique, offers incredible potential in ecological remediation such as the photodegradation of the organic pollutants in the wastewater Semiconductor photocatalysts such as SnO2 and SnO2 nano particles have pulled much attention in recent years due to their various applications to the photocatalytic degradation of organic pollutants in water and air and dye sensitized photovoltaic solar cell.[4] The interest is much more focused nowadays on the synthesis of photocatalyst materials to beat some limitations of the use of SnO2. Some of the important limitations are: SnO2 powder is hard to reuse, easy to agglomerate, and causes an issue of separation from the solution [5]. Many efforts have been paid to enhance the photocatalytic activity of semiconductor SnO2, such as semiconductor combination transition metal doping and noble metal deposition. Among these techniques doping with transition metals has been proved as effective strategies to enhance photo catalytic activity. In industrial wastewaters brought about in the textile industry, the heavy metals (cations or complexes), even in traces will adsorb on the photocatalyst surface. Cadmium is one of the presumable heavy metals in these wastewaters. It can be adsorbed on the active sites in processes of chemisorption or it can be integrated in the SnO2 lattice acting as a doping agent and immobilizing SnO2 on an innert and suitable supporting materials. For this reason several porous media used as far as possible, to provide a tremendous pore structure for dispersing SnO2 photocatalyst such as zeolite, alumina, silica, glass, carbon nano tube and activated charcoal.[6-10] Among these materials, activated charcoal is widely utilized as a support it gas and water remediation due to its good adsorption properties and seems to be an attractive support for SnO2. The increment in photocatalytic activity by the addition of charcoal has been well established. In this work, we report the preparation, characterization, photocatalytic and antibacterial activity of AC-supported Cd doped SnO2 nano composite materials. The obtained material was characterized by HR-SEM, with EDX, XRD, FT-RAMAN and PL Analysis. In the application part, we have studied their photocatalytic activity towards methylene blue in aqueous solution under UV light irradiation. In addition, we report antimicrobial activity of prepared AC-Cd/SnO2 nano composite materials using three gram positive and two gram negative bacterial strains and three antifungal strains, ciprofloxacin and Amphotericin used as a standard respectively. The results shown AC-Cd/SnO2 have higher bacterial and fungal activity than bare SnO2 and cd doped SnO2 nano material

MATERIAL AND METHODS

2.1 Materials

Two azo dye Methyl Green (MG) from Sigma Aldrich and the dyes were used without any further purification. The precursors such as titanium tetraisopropoxide (Lancaster, 97% pure), tetraethyl orthosilicate (Chemplast), stannous chloride pentahydrate, Cadmium acetate dihydrate, citric acid, activated charcoal, hydrochloric acid, sodium hydroxide, sulfuric acid and ethanol were used as received. Double distilled water was used throughout the photocatalytic studies. Chemicals peeled potato dextrose agar, peptone, sodium chloride, beef extract and yeast extract, distilled water were used for antibacterial and antifungal studies

2.2. Preparation of AC-supported Cd-doped SnO2 by precipitation method

AC-Supported Cd-doped SnO2 metal oxide was synthesized by precipitation method. Initially cadmium acetate dihydrate (0.2 M) and Activated charcoal were dissolved in anhydrous ethanol (solution A). 0.2 M citric acid and 0.4 M stannous chloride penta hydrates were in ethanol is taken as another solution B. The solution B is added to solution A and stirred well. To this 2 mL of NH4OH is added at room temperature under vigorous stirring until the precipitate formed. The obtained precipitate was washed with water and ethanol. Then the precipitate was collected and dried in oven at 100C for 12 h. The resulting powder was finally calcinated at 450C at 2 h in a muffle furnace to obtained AC-supported Cd-doped SnO2. The bare SnO2 was prepared without cadmium acetate di hydrate and activated charcoal. The Cd/SnO2 was prepared without activated charcoal

CHARACTERIZATION

High resolution Scanning Electron Microscopy (HRSEM) and Elementary Dispersive X-ray (EDX) analysis experiments were carried out on a FEI Quanta FEG 200 instrument with EDX analyzer facility at 25 8C. XRD spectra was recorded on the X'PERT PRO model X-ray diffractometer from Pan Analytical instruments operated at a voltage of 40 kV and a current of 30 mA with Cu Ka radiation. FT-RAMAN spectra were recorded with an integral microscope Raman system RFS27 spectrometer equipped with 1024 - 256 pixels liquefied nitrogen-cooled germanium detector. The 1064 nm line of the Nd:YAG laser (red laser) was used to excite. To avoid intensive heating of the sample, the laser power at the sample was not higher than 15 mW. Each spectrum was recorded with an acquisition time of 18 s. UV–vis (ultraviolet and visible light) absorbance spectra were measured over a range of 200–800 nm with a Shimadzu UV-1650PC recording spectrometer using a quartz cell with 10 mm of optical path length. Photoluminescence spectra at room temperature were recorded using a perkin-Elmer LS 55 fluorescence spectrometer. Nano particles were dispersed in chloroform and excited using light of wavelength 300nm.

RESULT AND DISCUSSION

4.1 FT-IR spectral analysis

FT-IR spectra in the range 4000-400 cm-1 of as synthesized metal oxides are shown in Fig.1a (a-c). The intense and broad bands of SnO2, Cd/SnO2 and AC-Cd/SnO2 at 3442-3439 and 1643-1624 cm-1 can be attributed to the O–H vibration in absorbed water on the sample surface. It is suggested that the high surface area of these nanostructured materials results in rapid adsorption of water from the atmosphere because the FT-IR samples were kept and ground in air. The broad bands between 850 and 422 cm-1 are attributed to the framework vibrations of the Sn–O bond in SnO2 [11-13]. The peak appeared at 636 cm-1 relates to the O–Sn–O bridge functional groups of AC-Cd/SnO2, which confirms the presence of SnO2 as crystalline phase.

4.2 FT-Raman spectral analysis

Figs.1.b (a-c) shows the Raman spectra of SnO2, Cd/SnO2 and AC-Cd/SnO2 metal oxides. Raman peaks at 475, 636 and 772 cm-1, corresponding to the Eg, A1g and B2g vibration modes were observed, respectively. Thus, these peaks further confirm that the as-synthesized SnO2 possess the characteristics of the tetragonal rutile structure [14]. Raman spectra peaks at 1402 and 1605 cm-1 can be ascribed to D and G bands of carbon, respectively.

4.3 Photoluminescence Spectral Analysis

PL spectra of prepared SnO2, Cd/SnO2 and AC-Cd/SnO2 are shown in Figs. 5.1.7(a-c). The photoluminescence emission spectra of SnO2 metal oxide at 296 nm excitation and catalyst exhibit emission at 365 and 420 nm. The emission band at 365 nm can be attributed to electron transition mediated by defects levels in the band gap, such as oxygen vacancies. The emission maximum of 420 nm is lower than the band gap of the SnO2 bulk, this peak can be attributed to the contribution of oxygen vacancies and defect in the SnO2 nanoparticles [15].

4.4 XRD analysis

Figs.2b(a-c) shows the X-ray diffraction patterns of SnO2, Cd/SnO2 and AC-Cd/SnO2, respectively. The XRD pattern of undoped SnO2 shows the peaks at 2θ = 33.6, 37.4, 38.2, 51.8 and 65.2 are the characteristic diffractions of the (002), (101), (200), (211) and (301) planes, respectively, which match with the tetragonal rutile structure of SnO2. The sharp diffraction peak at (110) plane for the samples SnO2, Cd/SnO2 and AC-Cd/SnO2 metal oxides indicates the preferred crystallite growth in the particular direction [16-19]. However, the presence of diffraction peaks with a value of 2θ around 21.6 relative to the (002) plane (JCPDS Card No. 50 0927) is assigned as graphite oxide and graphite carbon (Fig. 2b(c). The peaks corresponding to Cd/TiO2 metal oxide at 2θ = 35.52 relative to the (111) plane, could be observed [Figs. 2b (b and c)]. The size of Cd/SnO2 and AC-Cd/SnO2 metal oxide was distributed mainly in the range of 3-5 nm and the average size of Cd/SnO2 and AC-Cd/SnO2 metal oxides being about 4 nm.

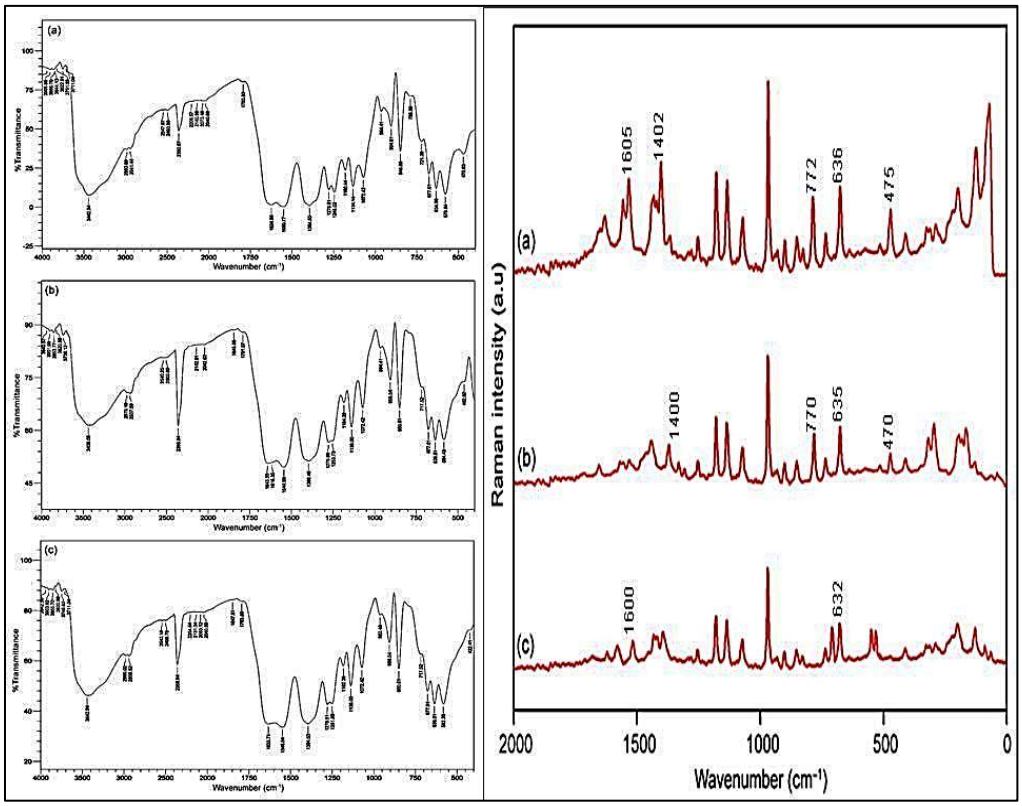

Figure:1 FT-IR and FT-Raman spectral analysis of SnO2, Cd/SnO2 and AC-Cd/SnO2

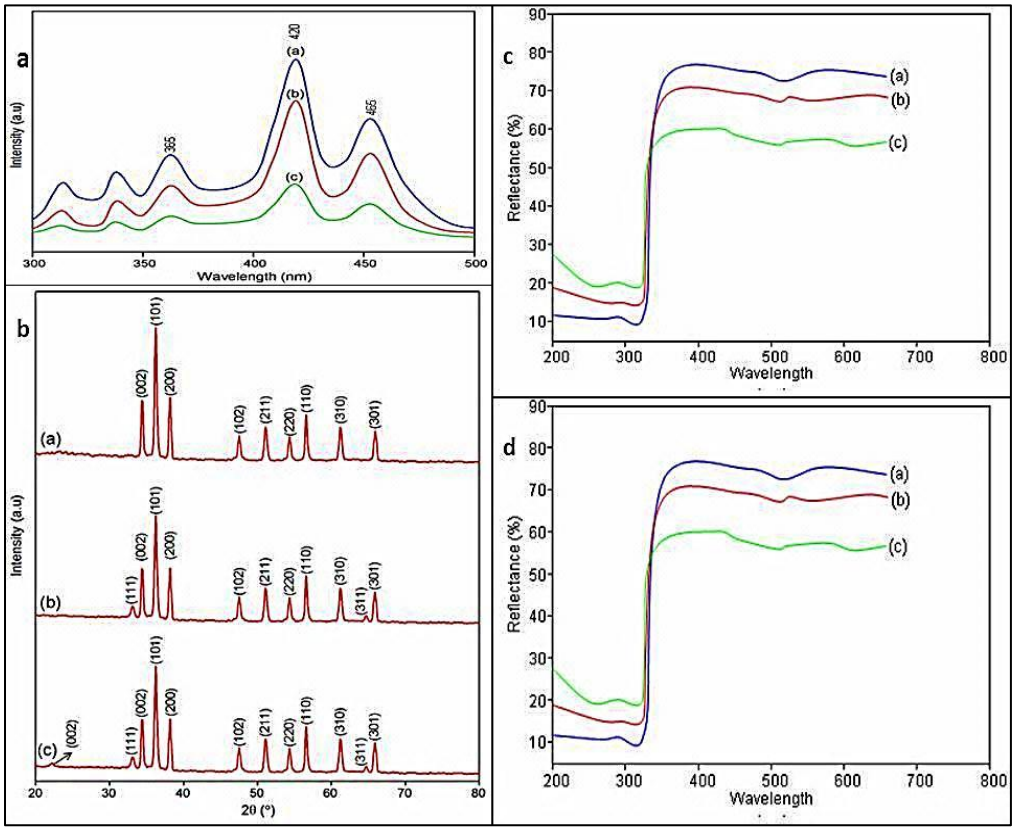

Figure:2 (a)PL, (b)XRD and (c&d) DRS analysis of SnO2, Cd/SnO2 and AC-Cd/SnO2

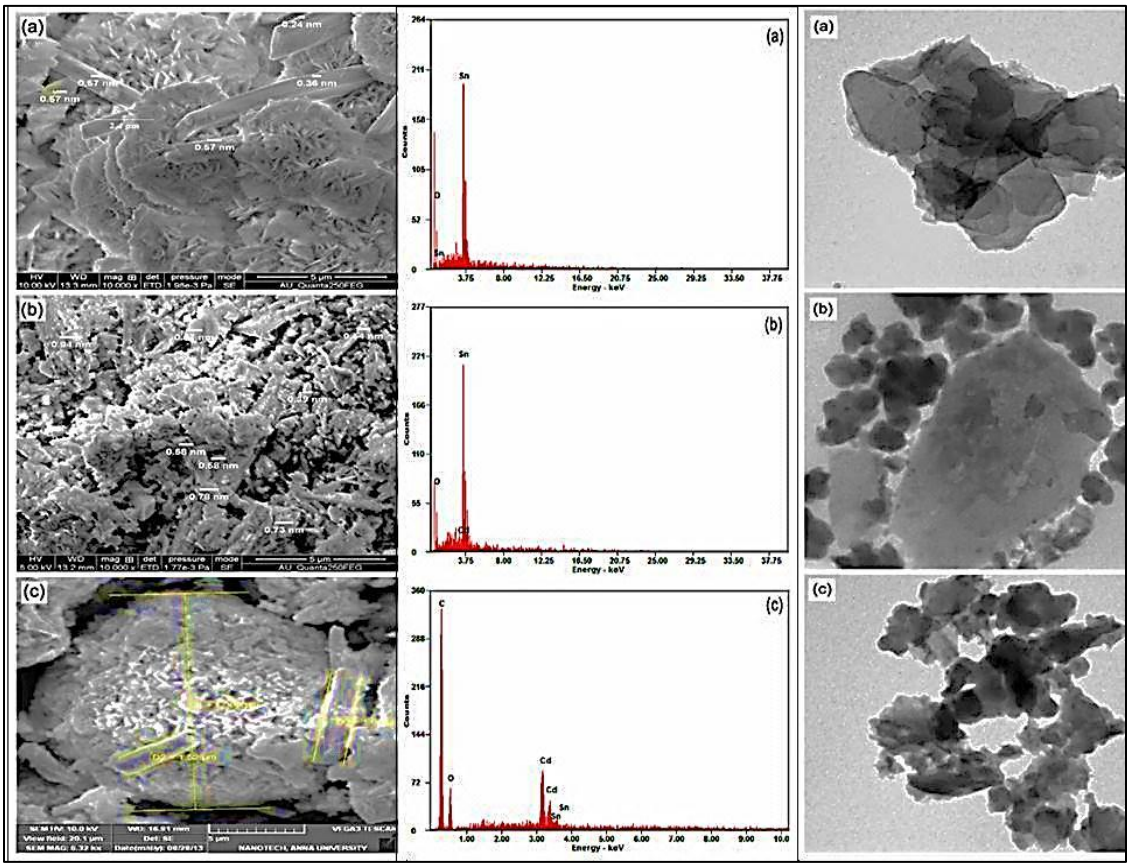

Fgure:3 SEM, EDS and TEM Analysis of SnO2, Cd/SnO2 and AC-Cd/SnO2

4.5 Diffuse reflectance spectral (DRS) analysis

The Kubelka-Munk plots obtained from the DRS spectra of pure SnO2, Cd/SnO2 and AC-Cd/SnO2 are shown in Fig. 2c & 2d. The optical reflectance spectra depend on several factors, such as band gap, oxygen deficiency, surface roughness and impurity centers. The spectra show cut-off regions in a specific wavelength range, which can be attributed to the photoexcitation of electrons from valence band to conduction band. The optical absorbance can be approximately calculated from the from the optical reflectance data by the Kubelka-Munk function [20], The measured band gap was found to be 3.60 eV for undoped SnO2. This can be attributed to the quantum confinement effect in the samples [21]. On doping with cadmium, the band gap energy decreases, 3.55 eV for Cd/SnO2 and 3.48 eV for AC-Cd/SnO2 (Fig. 2c & 2d). The formation of sub-bands in between the conduction band and sub-bands are merging with the conduction band to form a continuous band [22] due to the doping effect of cadmium and activated charcoal in tin oxide matrix.

4.6 SEM Analysis

The Surface morphology of SnO2, Cd/SnO2 and AC-Cd/SnO2 has been studied using high-resolution scanning electron microscope. Figs. 3a(a-c) shows the HR-SEM images of the as prepared SnO2, Cd/SnO2 and AC-Cd/SnO2. The metal oxides were seem to various shape and the diameter of about 50-75 nm was clearly observed. SEM images of SnO2 show the existence of rod and flower like crystalline metal oxides (Fig. 5.1.2a) was showed that metal oxides are agglomerated due to drying and calcinations process. Figs. 3a(b and c) shows the HR-SEM images of Cd/SnO2 and AC-Cd/SnO2 metal oxides[23]. These images confirm the existence of nanorod, sheet and highly agglomerated spherical metal oxides.

4.7 EDS analysis

Figs. 3b(a-c) shows the EDS images of the prepared SnO2, Cd/SnO2 and AC-Cd/SnO2. The EDS spectrum is used to confirm the composition of the prepared catalysts. In Figs. 3b (a-c) confirm the catalysts (SnO2, Cd/SnO2 and AC-Cd/SnO2) contains Sn, O, and Sn, O, Cd and Sn, O, Cd, C,

respectively [24-25]. The EDS pattern of the sample is indicates that high purity, which is in good agreement with the XRD.

4.8 TEM Analysis

Figs.3c (a-c) shows the TEM images of the SnO2, Cd/SnO2 and AC-Cd/SnO2. Fig. 5.1.4a reveals that most of the particles has uneven hexagonal sheets. Fig. 5.1.4b shows nanosheets with some dark black shadow like sticking onto the surface and this may be due to the presence of Cd. However, a slight aggregation of particles has been observed in the AC-Cd/SnO2. It is observed that metal oxides have a narrow size distribution [26]. Moreover, the particle sizes of all the samples obtained from TEM patterns quite similar to those calculated from Scherer's equation.

PHOTO DEGRADATION OF METHYL GREEN (MG) ON SNO2, CD/SNO2 AND AC-CD/SNO2 UNDER UV LIGHT

5.1. Primary analysis

The photodegradability and decolourization of MG with SnO2, Cd/SnO2 and AC-Cd/SnO2 metal oxides under UV light irradiation is shown in Fig. 4a & b. Almost 96.2% of degradation and 95.4% of decolourization of the dye takes place at a time of 60 min with AC-Cd/SnO2 under UV light. The catalysts SnO2 and Cd/SnO2 were used under the same conditions, 72% and 88.4% of degradation and 78.5 and 88.2% of decolourization occurred at 60 min. This shows that AC-Cd/SnO2 is more efficient in MG dye degradation and decolourization than other catalysts. It was observed that there was a decrease in absorbance of MG dye solution with increasing time of exposure. In the present case, the degradation followed the first-order reaction kinetics.

5.2. Effect of solution pH

The effect of pH on the photodegradation of MG was studied in the pH range 3-11 after 60 min of irradiation are shown in Fig.4c. The pseudo first-order rate constants for AC-Cd/SnO2 at pH 3, 5, 7, 9 and 11 are and 0.0282, 0.0286, 0.0288, 0.0285 and 0.0283 min-1, respectively. It is observed that the increase in pH from 3 increases the removal efficiency of methyl green dye up to pH 7 and then decreases. The optimum pH for efficient MG removal on AC-Cd/SnO2 is 7. Above pH 7, the photocatalytic degradation of MG rapidly decreases. Reason for this effect has been discussed earlier (section 5.2.2).

5.3. Effect of catalyst loading

Experiments performed with different amounts of AC-Cd/SnO2 showed that the photo degradation efficiency increased with an increase in amount up to 0.08 g/50mL and then slightly decrease as observed in Fig. 4d. The pseudo-first order rate constants are 0.0282, 0.0285, 0.0288, 0.0285 and 0.0282 min-1 for AC-Cd/SnO2 at catalyst loadings of 0.04, 0.06, 0.08, 0.1 and 0.12 g/50 mL, respectively. The constancy at higher catalyst loading beyond the optimum level of 0.08 g/50mL shown in Fig 5.3.3. Reason for this effect has been discussed earlier (section 5.2.3).

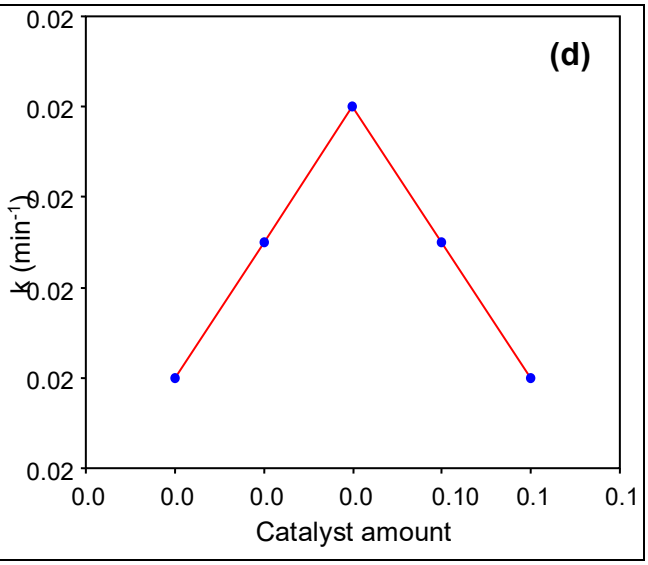

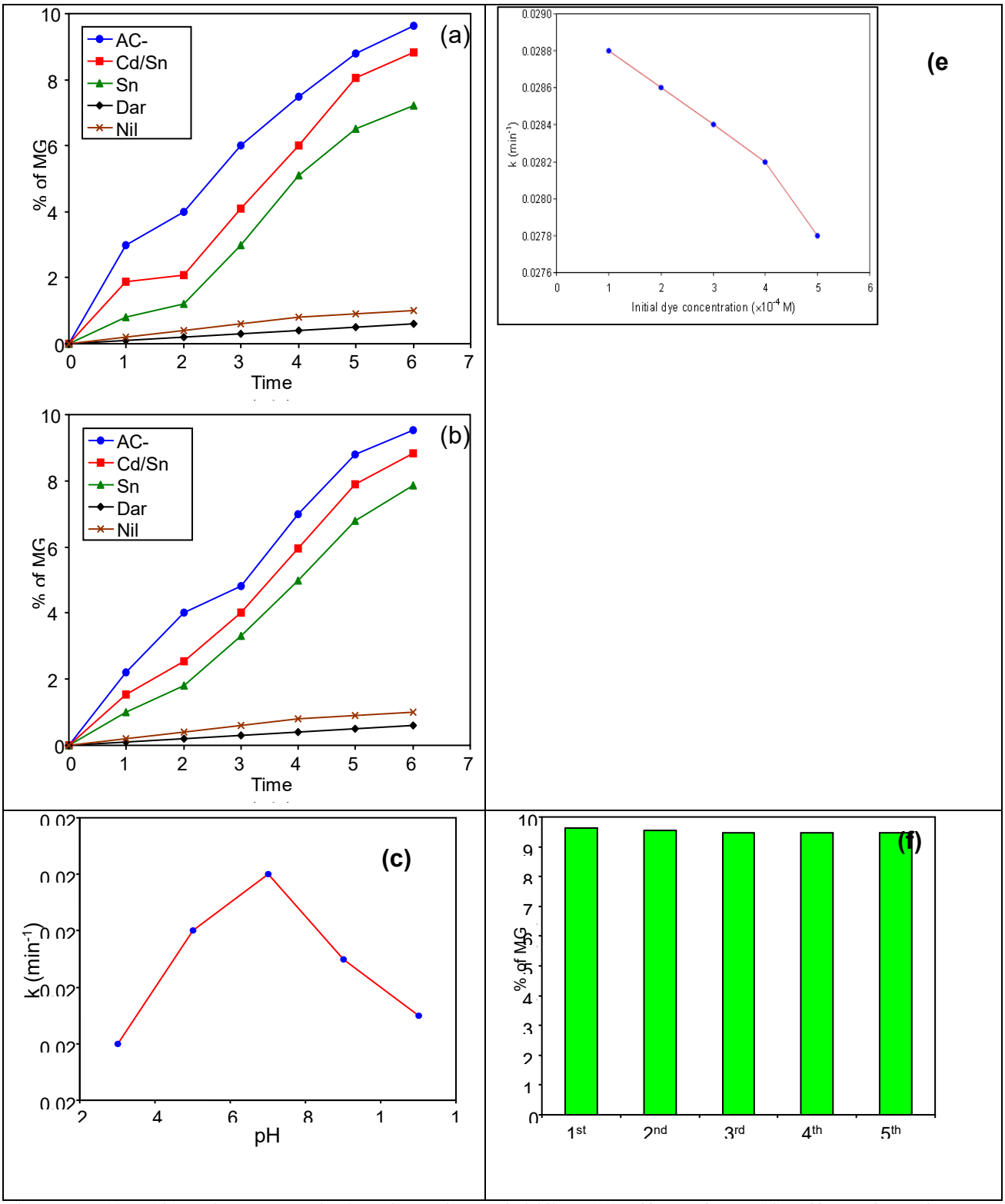

Figure:4 (a) & (b) Primary analysis, Photodegradability, (c) Effect of pH, (d) Effect of catalyst loading (e) Effect of initial dye concentration and (f) Effect of reusability of Methyl green(MG)

5.4. Effect of initial dye concentration

Different concentrations of MG were prepared and it is used for the photodegradation and decolourization process by using UV light. Photodegradation and decolourization of MG was high in lower concentration when compared to of it higher concentration. Fig. 4e shows that the increase of dye concentration from 1 to 5 10-4 M decreases the rate constant from 0.0288 to 0.0278 min-1. However on increasing the concentration above 1 10-4 M, the reaction rate was found to decrease. Reason for this effect has been discussed earlier (section 5.2.4).

5.5. Effect of reusability

The reusability of the AC-Cd/SnO2 photocatalyst was investigated by repeating MG degradation experiments five times. Almost complete degradation occurred in the 1st, 2nd, 3rd, 4th and 5th run obtained 96.2, 95.5, 94.8, 94.8 and 94.8% degradation (Fig.4f). There is no change in the degradation efficiency of AC-Cd/SnO2 after third run. The results indicate prepared catalysts are stable and reusable. Thus suggests that AC-Cd/SnO2 photocatalysts have excellent stability and reliability for photodegradation of pollutants.

5.6. Mechanism of dye degradation

$$AC\text{-}Cd/SnO_2 + h\nu \longrightarrow e^-_{CB} + h^+_{VB} \quad \ldots (5.1)$$

$$H_2O + h^+_{VB} \longrightarrow OH^\cdot + H^+ \quad \ldots (5.2)$$

$$O_2 + e^-_{CB} \longrightarrow O_2^{\cdot -} \quad \ldots (5.3)$$

$$O_2^{\cdot -} + H^+ \longrightarrow HO_2^\cdot \quad \ldots (5.4)$$

$$2HO_2^\cdot \longrightarrow H_2O_2 + O_2 \quad \ldots (5.5)$$

$$H_2O_2 + O_2^{\cdot -} \longrightarrow OH^\cdot + O_2 + OH^- \quad \ldots (5.6)$$

$$OH^\cdot + MG^+ \longrightarrow \text{Degraded product} \quad \ldots (5.7)$$

AC-Cd/SnO2 can absorb UV light and generate electron-hole pairs. These photogenerated electron and hole pairs can migrate into the catalyst surface and react with surface adsorbed O2 to form O2•−. In absence of O2 these electrons and holes will recombine. The O2•− can react with surface adsorbed H2O to form H2O2 which is responsible for generation of OH radical[27-30]. The OH is a potent indiscriminant oxidizing agent which possibly responsible for degradation of most of the surface adsorbed MG. The h+ can also react with the surface adsorbed H2O to form OH radical.

The degradation of MG dye to produce less toxic or harmless products is a green chemical approach to wastewater treatment.

5.5. antimicrobial studies

5.5.1. Antibacterial activity

The synthesized metal oxides SnO2, Cd/SnO2 and AC-Cd/SnO2 were screened for the antibacterial activity against two Gram-positive bacteria *viz., Bacillus subtilis* and *Staphylococcus aureus* and two Gram-negative bacteria *viz., Escherichia coli* and *Pseudomonas aeruginosa* by using the disc diffusion method. Ciprofloxacin (10 g/disc) antibacterial positive control produced the mean zone of inhibition ranged from 24 to 25 mm.

The zones of inhibition values are given in Table.1 and the antibacterial activity of the metal oxides SnO2, Cd/SnO2 and AC-Cd/SnO2 are shown in Fig:5 showed SnO2, Cd/SnO2 and AC-Cd/SnO2 metal oxides were possessed significant activity almost potential with the standard Ciprofloxacin against bacterial strains[31-32]. Thus the particle size places a vital role of imparting enhanced antibacterial activity to the metal oxides.

Table 1.Antibacterial activity of SnO2, Cd/SnO2 and AC-Cd/SnO2 nonmaterials by disc diffusion method

S. No.	Name of the bacterial strains	Ciprofloxacin (10 μg/disc)	Zone of inhibition (mm)		
			SnO_2	Cd/SnO_2	$AC\text{-}Cd/SnO_2$
1	*Bacillus subtilis*	24	13	15	23
2	*Staphylococcus aureus*	24	12	14	22
3	*Escherichia coli*	25	12	14	21
4	*Pseudomonas aeruginosa*	25	12	13	20

The screening results indicate that the compound AC-Cd/SnO2 was found to be active against *B. subtilis* (23 mm), *S. aureus* (22 mm), *E. coli* (21 mm) and *P. aeruginosa* (20 mm) at the same concentration of metal oxides SnO2 and Cd/SnO2 were found to be moderately active against *B. subtilis*, *S. aureus*, *E. coli* and *P. aeruginosa*.

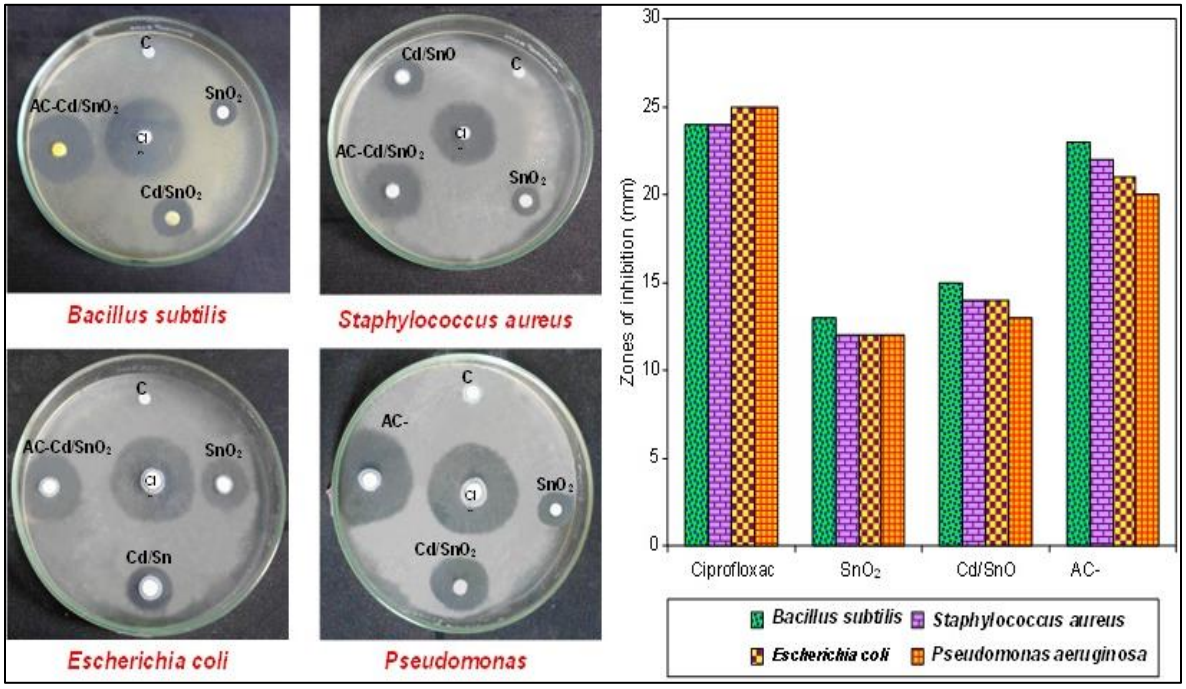

Figure 5. Antibacterial activity of SnO2, Cd/SnO2 and AC-Cd/SnO2 by disc diffusion method

5.5.2. Antifungal activity

The disc method was employed for the *in vitro* study of antifungal effects against *Aspergillus flavus, Aspergillus niger* and *Trichoderma viride*.

Table.2.Antifungal activity of SnO2, Cd/SnO2 and AC-Cd/SnO2 by disc diffusion method

S. No.	Name of the fungal strains	Amphotericin-B (100 units/disc)	Zone of inhibition (mm)		
			SnO_2	Cd/SnO_2	$AC\text{-}Cd/SnO_2$
1	*Aspergillus flavus*	28	16	18	24
2	*Aspergillus niger*	23	11	13	19
3	*Trichoderma viride*	25	13	17	22

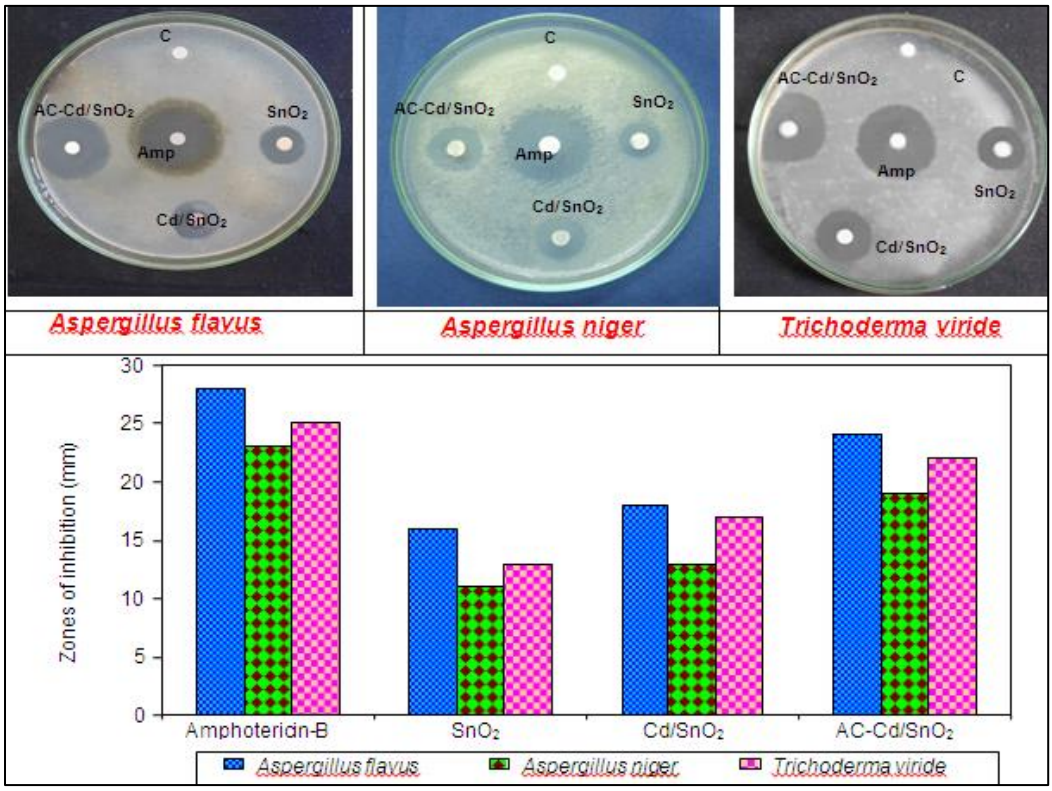

Figure:6 Antifungal activity of SnO2, Cd/SnO2 and AC-Cd/SnO2 by disc diffusion method. C – Control; Amp. – Amphotericin-B (as standard)

The antifungal activity of the SnO2, Cd/SnO2 and AC-Cd/SnO2 metal oxides are shown in Fig.6 and the zones of inhibition values are given Table 5.5.2. The photographs showed the synthesized metal oxides SnO2, Cd/SnO2 and AC-Cd/SnO2 were screened for the antifungal activity against, *A. flavus*, *A. niger* and *T. viride* (Fig. 5.5.4). Amphotericin-B (100 units/disc) antifungal positive control produced the mean zones of inhibition ranged from 23 to 28 mm.

Thus the particle size places a vital role of imparting enhanced antifungal activity to the metal oxides. The screening results indicate that the compound AC-Cd/SnO2 was found to be active against *A. flavus* (24 mm), *A. niger* (19 mm) and *T. viride* (22 nm). At the same time metal oxides SnO2 and Cd/SnO2 were found to moderately active against *A. niger* and *T. viride*.

CONCLUSION

AC Supported cadmium doped SnO2 nanocomposite material was prepared by a precipitation method .This material was characterized by powder X-ray diffraction (XRD) , high resolution scanning electron micrographs(HRSEM) with energy dispersive X-ray analysis, photoluminescence (PL) and Fourier transform Raman analysis(FT-RAMAN).These results confirmed the formation of AC-Cd/SnO2 nanocomposite material.HR SEM and XRD analysis of SnO2 and Cd/SnO2 showed the average size of as 12.3 nm, AC-Cd/SnO2 showed the average particle size of as 5 nm. Moreover the decrease in particle size can be correlated with increase of the surface area .The EDX shows the presence of C and Cd in the SnO2 material. XRD reveal the all strong peaks can be indexed as Hexagonal wurzite form of SnO2. PL Spectra explain the suppression of recombination of the photogenerated electron hole pairs by AC-Cd/SnO2 nano material. AC-Cd/SnO2 reveals enhanced photocatalytic activities as compared to SnO2 and Cd/SnO2 for the photodegradation and decolourization of MG under UV light irradiation for 0 to 60 minutes. The mechanism of photo catalytic effect of AC-Cd/SnO2 nano composite material has been discussed.

REFERENCE

1. Zhang, D.; Zeng, F. *Journal of Materials Science*, **47** (2012) 2155–2161. https://doi.org/10.1007/s10853-011-6016-4

2. Faisal, M.; Ismail, A. A.; Ibrahim, A. A.; Bouzid, H.; Al-Sayari, S. A. *Chemical Engineering Journal*, **229** (2013) 225–233. https://doi.org/10.1016/j.cej.2013.06.004
3. Singh, P.; Ahn, S.; Kang, J.; Veronika, S.; *et al. Artificial Cells, Nanomedicine, and Biotechnology*, **46** (2018) 2022. https://doi.org/10.1080/21691401.2017.1408117
4. Chandrabose, V. L.; Natanapatham, L.; Karthikeyan, B.; Kamalakkannan, J.; Prabha, S.; Senthilvelan, S. *Materials Research Bulletin*, **48** (2013) 3707–3712. https://doi.org/10.1016/j.materresbull.2013.05.121
5. Slimen, H.; Houas, A.; Nogier, J.-P. *Journal of Photochemistry and Photobiology A: Chemistry*, **221** (2011) 13–21. https://doi.org/10.1016/j.jphotochem.2011.04.013
6. Shankar, M. V.; Anandan, S.; Venkatachalam, N.; Arabindoo, B.; Murugesan, V. *Chemosphere*, **63** (2006) 1014–1021. https://doi.org/10.1016/j.chemosphere.2005.08.041
7. Zhang, X.; Zhou, M.; Lei, L. *Applied Catalysis A: General*, **282** (2005) 285–293. https://doi.org/10.1016/j.apcata.2004.12.022
8. Yazawa, T.; Machida, F.; Kubo, N.; Jin, T. *Ceramics International*, **35** (2009) 3321–3325. https://doi.org/10.1016/j.ceramint.2009.05.029
9. Yu, Y.; Yu, J. C.; Yu, J.-G.; Kwok, Y.-C.; Che, Y.-K.; Zhao, J.-C.; Ding, L.; Ge, W.-K.; Wong, P.-K. *Applied Catalysis A: General*, **289** (2005) 186–196. https://doi.org/10.1016/j.apcata.2005.04.057
10. Tryba, B.; Morawski, A. W.; Inagaki, M. *Applied Catalysis B: Environmental*, **41** (2003) 427–433. https://doi.org/10.1016/S0926-3373(02)00173-X
11. Ahmad, S. *Journal of Physics: Conference Series*, **755** (2016) 011001. https://doi.org/10.1088/1742-6596/755/1/011001
12. Kuantama, E.; Han, D.-W.; Sung, Y.-M.; Song, J.-E.; Han, C.-H. *Thin Solid Films*, **517** (2009) 4211–4214. https://doi.org/10.1016/j.tsf.2009.02.044
13. Shi, L.; Lin, H. *Langmuir*, **26** (2010) 18718–18722. https://doi.org/10.1021/la103769d
14. Wang, W. Z.; Xu, C. K.; Wang, G. H.; Liu, Y. K.; Zheng, C. L. *Journal of Applied Physics*, **92** (2002) 2740. https://doi.org/10.1063/1.1497718
15. Gu, F.; Wang, S. F.; Lu, M. K.; Qi, Y. X.; Zhou, G. J.; Xu, D.; Yuan, D. R. *Inorganic Chemistry Communications*, **6** (2003) 882–885. https://doi.org/10.1016/S1387-7003(03)00135-7
16. Ding, S.; Chen, J. S.; Qi, G.; Duan, X.; Wang, Z.; Giannelis, E. P.; Archer, L. A.; Lou, X. W. *Journal of the American Chemical Society*, **133** (2011) 21–23. https://doi.org/10.1021/ja108720w
17. Liu, C. M.; Fang, L. M.; Zu, X. T.; Zhou, W. L. *Physica Scripta*, **80** (2009) 065703. https://doi.org/10.1088/0031-8949/80/06/065703
18. Liu, X.; Wang, X.; Peng, L.; Sun, Z. *Surface and Coatings Technology*, **201** (2007) 7607–7614. https://doi.org/10.1016/j.surfcoat.2007.02.004
19. Zhang, J.; Gao, L. *Journal of Solid State Chemistry*, **177** (2004) 1425–1430. https://doi.org/10.1016/j.jssc.2003.11.024
20. Fan, G.; Gu, Z.; Yang, L.; Li, F. *Chemical Engineering Journal*, **155** (2009) 534–540. https://doi.org/10.1016/j.cej.2009.08.008
21. Takagahara, T.; Takeda, K. *Physical Review B*, **46** (1992) 15578. https://doi.org/10.1103/PhysRevB.46.15578
22. Ahmed, J.; Saha, S.; Trinh, G. P.; Mugweru, A. M.; Ramanujachary, K. V.; Lofland, S. E.; Ganguli, A. K. *Journal of Physical Chemistry C*, **115** (2011) 14526.
23. Chen, K. J.; Hung, F. Y.; Chen, Y. T.; Chang, S. J.; Hu, Z. S. *Materials Transactions*, **51** (2010) 1340. https://doi.org/10.2320/matertrans.M2009378
24. Berumen-Torres, J. A.; Quinones-Galvan, J. G.; Duran-Munoz, H.; Guzman, C. H.; *et al. Materials Science and Engineering B*, **268** (2021) 115134. https://doi.org/10.1016/j.mseb.2021.115134
25. Khandelwal, A.; Shukla, R.; Sharma, K. S. *Journal of Scientific Research*, **16** (1) (2024) 41–51. https://doi.org/10.3329/jsr.v16i1.64157

26. Satheesh, A.; Rao, J. C.; Ramanjaneyulu, M. V. V.; Jogayya, K. N.; Kalyan, K. V.; Kumar, A.; Usha, H. *Journal of Scientific Research*, **16** (2) (2024) 561–573. https://doi.org/10.3329/jsr.v16i2.69301
27. Girija, R.; Mary, S. S.; Balakrishnan, G.; Mariappan, S. M.; Hamdy, M. S.; Shkir, M. *ChemistrySelect*, **7** (2022) e202103614. https://doi.org/10.1002/slct.202103614
28. Le, H. A.; Linh, L. T.; Chin, S.; Jurng, J. *Powder Technology*, **225** (2012) 167–175. https://doi.org/10.1016/j.powtec.2012.04.004
29. Wu, R.-J.; Chen, C.-C.; Lu, C.-S.; Hsu, P.-Y.; Chen, M.-H. *Desalination*, **250** (2010) 869–875. https://doi.org/10.1016/j.desal.2009.03.026
30. Wang, G.; Wu, F.; Zhang, X.; Luo, M.; Deng, N. *Journal of Hazardous Materials*, **133** (2006) 85–91. https://doi.org/10.1016/j.jhazmat.2005.09.058
31. Muhammad, M. H.; Idris, A. L.; Fan, X.; Guo, Y.; Yu, Y.; Jin, X.; Qiu, J.; Guan, X.; Huang, T. *Frontiers in Microbiology*, **11** (2020) 928. https://doi.org/10.3389/fmicb.2020.00928
32. Singh, Y.; Saxena, M. K. *Frontiers in Microbiology*, **13** (2022) 982611. https://doi.org/10.3389/fmicb.2022.982611

